AGU PUBLICATIONS

JGR

Journal of Geophysical Research: Earth Surface

RESEARCH ARTICLE
10.1002/2015JF003637

Key Points:
- Flow separation occurrence, extent, and magnitude decrease with dune lee slope
- Low-angle dunes exhibit weaker shear layer and lower turbulence production
- There is a nonlinear decrease in flow resistance with dune lee slope

Correspondence to:
E. Kwoll,
eva_kwoll@sfu.ca

Citation:
Kwoll, E., J. G. Venditti, R. W. Bradley, and C. Winter (2016), Flow structure and resistance over subaquaeous high- and low-angle dunes, *J. Geophys. Res. Earth Surf.*, *121*, doi:10.1002/2015JF003637.

Received 10 JUN 2015
Accepted 15 FEB 2016
Accepted article online 18 FEB 2016

Flow structure and resistance over subaquaeous high- and low-angle dunes

E. Kwoll[1,2], J. G. Venditti[2], R. W. Bradley[2], and C. Winter[1]

[1]MARUM-Center for Marine Environmental Sciences, University of Bremen, Bremen, Germany, [2]Department of Geography, Simon Fraser University, Burnaby, British Columbia, Canada

Abstract A prominent control on the flow over subaqueous dunes is the slope of the downstream leeside. While previous work has focused on steep (~30°), asymmetric dunes with permanent flow separation, little is known about dunes with lower lee slope angles for which flow separation is absent or intermittent. Here we present a laboratory investigation where we systematically varied the dune lee slope, holding other geometric parameters and flow hydraulics constant, to explore effects on the turbulent flow field and flow resistance. Three sets of fixed dunes (lee slopes of 10°, 20°, and 30°) were separately installed in a 15 m long and 1 m wide flume and subjected to 0.20 m deep flow. Measurements consisted of high-frequency, vertical profiles collected with a Laser Doppler Velocimeter. We show that the temporal and spatial occurrence of flow separation decreases with dune lee slope. Velocity gradients in the dune leeside depict a free shear layer downstream of the 30° dunes and a weaker shear layer closer to the bed for the 20° and 10° dunes. The decrease in velocity gradients leads to lower magnitude of turbulence production for gentle lee slopes. Aperiodic, strong ejection events dominate the shear layer but decrease in strength and frequency for low-angle dunes. Flow resistance of dunes decreases with lee slope; the transition being nonlinear. Over the 10°, 20°, and 30° dunes, shear stress is 8%, 33%, and 90% greater than a flat bed, respectively. Our results demonstrate that dune lee slope plays an important but often ignored role in flow resistance.

1. Introduction

In sand-bedded rivers, estuaries, and coastal environments, bed forms take on a variety of shapes and scales, as they form through the interaction of the mobile sandy bed and turbulent flow field. Dunes, in particular, have been subject to extensive research due to their significance in controlling hydraulic roughness and sediment transport (see reviews in *Best* [2005], *Coleman and Nikora* [2011], and *Venditti* [2013]). A morphological difference has been observed between small-scale dunes formed in shallow and deep flows [*Kostaschuk*, 2006]. Shallow flows produce dunes with an asymmetric shape and a steep angle-of-repose leeside of ~30° ("high-angle dunes") [e.g., *Schindler and Robert*, 2005; *Venditti et al.,* 2005; *Wren et al.,* 2007; *Naqshband et al.,* 2014], while in deep rivers and estuaries, dunes typically have much lower angle lee slopes (average lee slopes between 5° and 12°, "low-angle dunes") and more symmetric shapes [*Smith and McLean*, 1977; *Kostaschuk and Villard*, 1996, 1999; *Roden*, 1998; *Carling et al.,* 2000b; *Bradley et al.,* 2013; *Hendershot et al.,* 2016]. Following *Kostaschuk* [2006], we refer to all dunes with a lee slope $\geq 30°$ as high-angle and dunes with lee slopes $<30°$ as low-angle.

The exact cause of these differing morphologies remains unclear. While low-angle dunes have not been produced in laboratory flows, high-angle dunes do occur in deep flows [cf. *Roden*, 1998; *Hendershot et al.,* 2016], so flow depth does not appear to be the controlling variable. However, the dominant mechanism of sediment transport appears to be important. Low-angle dunes are often attributed to the higher transport rates of bed material in suspension relative to bed load transport in large channels [*Smith and McLean*, 1977; *Kostaschuk and Villard*, 1996; *Kostaschuk et al.,* 2009]. Dune heights and steepness have been shown to decrease with increasing suspended/bed load transport ratio due to crestal erosion under high shear stresses [*Fredsøe*, 1981; *Amsler and Schreider*, 1999; *Kostaschuk*, 2006]. High concentrations of suspended sediment may lead to an excess sediment supply to the dune leeside where it is deposited creating a less steep lee slope [*Smith and McLean*, 1977; *Kostaschuk and Villard*, 1996; *Kostaschuk et al.,* 2009]. *Hendershot et al.* [2016] showed a systematic variation in the dune leeside coincident with changes in suspended sediment concentrations in the water column. *Best and Kostaschuk* [2002] have made analogies between the morphologic adaptation of dunes and the transition to upper stage plane bed conditions [*Saunderson and Lockett*,

1983; *Bridge and Best*, 1988]. Damping of turbulence under high suspension flows has been linked to increased deposition and lower lee slopes [*Bridge and Best*, 1988; *Best*, 1996]. Experiments on the behavior of dunes in high clay concentration flows have produced flatter dune morphologies as a result of turbulence suppression [*Wan and Wang*, 1994].

Dune morphology is also intrinsically linked to fluid dynamics in so far as the lee slope controls whether flow separation and reversal will occur above the lee and crest of a dune [*Smith and McLean*, 1977; *Kostaschuk and Villard*, 1996; *Carling et al.,* 2000b; *Best and Kostaschuk*, 2002; *Sukhodolov et al.,* 2006]. The flow field associated with high-angle dunes exhibiting permanent flow separation has been studied extensively [e.g., *Nelson et al.,* 1993; *McLean et al.,* 1994; *Bennett and Best*, 1995; *Venditti and Bennett*, 2000; *Venditti*, 2007] and is reasonably well understood; rapid flow expansion and deceleration downstream of the dune crest causes formation of a permanent region of flow separation and reversal above the dune leeside and trough region. A separated shear layer borders the region of flow reversal and reattaches 4–6 dune heights (*H*) downstream. An internal boundary layer (IBL) develops downstream of reattachment with increasing vertical extent toward the crest (see reviews in *Best* [2005], *Coleman and Nikora* [2011], and *Venditti* [2013].

Understanding of the flow field above low-angle dunes, however, remains limited due to a lack of detailed measurements and comparability between dune morphologies and flow conditions. Several field studies indicate that the flow separation region observed over high-angle dunes is replaced by a flow deceleration region with a smaller zone of intermittent flow reversal [*Roden*, 1998; *Carling et al.,* 2000b], while others have observed no flow reversal [*Smith and McLean*, 1977; *Kostaschuk and Villard*, 1996; *Sukhodolov et al.,* 2006; *Shugar et al.,* 2010; *Bradley et al.,* 2013]. Field studies, however, are subject to inherent difficulties in measuring close to the bed [*Kostaschuk et al.,* 2005; *Parsons et al.,* 2005], which may limit detection capabilities of flow separation downstream of low-angle dunes.

Best and Kostaschuk [2002] provided the most detailed set of observations of flow over fixed, low-angle dunes (14°) scaled after morphology observed from the Fraser River, British Columbia. They show that the separation region observed over high-angle dunes is absent over a low-angle dune. A decelerated flow region develops in the lee with a smaller zone of intermittent flow reversal. Upstream flow over the low-angle dune only occurred for 4% of the time. Later work by *Sukhodolov et al.* [2006] observed no evidence of flow separation downstream of laboratory dunes with a lee slope of 12°. *Motamedi et al.* [2012, 2014] investigated flow over gravel dunes in laboratory flows with lee slopes of 8°. They observed no permanent flow separation but did not consider intermittent separation. So it remains uncertain at what critical lee slope the onset of flow separation occurs and how lee slope angle affects flow separation intermittency.

Laboratory and numerical investigations of water and air flow over geometrically similar sinusoidal waves, bluff bodies, and negative steps have revealed some of the limiting conditions on flow separation. *Zilker and Hanratty* [1979] showed that the critical slope for the onset of intermittent separation over sinusoidal waves was lower for small Reynolds numbers. It has also been shown that flow separation in air over sinusoidal hills is suppressed above smooth hill surfaces [*Britter et al.,* 1981; *Wood*, 1995; *Gong et al.,* 1996; *Cao and Tamura*, 2006]. This suggests that the variety of critical slopes reported for flow separation downstream of dunes may stem from Reynolds number effects and differences in bed roughness. This argues for a systematic study of flow separation, where dune geometry, Reynolds number, surface roughness, and hydraulics are held constant, and only the lee slope angle is varied. Some work of this type has been undertaken. *Ruck and Makiola* [1990] systematically studied the effect of the slope of a negative step on flow separation in a wind tunnel, revealing that permanent flow separation occurred for lee slopes $\geq$15°. Unfortunately, they did not explore intermittent separation. Nor is it obvious how these results can be abstracted to a low-angle dune. As such, it remains necessary to explore how intermittent flow separation varies when dune lee slope is the only variable changed.

Over dunes, permanent flow separation is often associated with high macroturbulence production along the separated shear layer and at flow reattachment that cause a momentum deficit advected downstream in a wake structure [e.g., *Nelson et al.,* 1993; *McLean et al.,* 1994; *Bennett and Best*, 1995; *Venditti and Bennett*, 2000; *Venditti*, 2007]. Turbulence production takes the form of large-scale turbulent flow structures that may surface as boils [*Matthes*, 1947; *Jackson*, 1976] and are responsible for moving large volumes of bed

material in suspension [*Rood and Hickin*, 1989; *Kostaschuk*, 2000; *Venditti and Bennett*, 2000]. However, large-scale suspension events have also been observed over low-angle dunes without permanent flow separation [*Kostaschuk and Church*, 1993; *Kostaschuk and Villard*, 1999; *Bradley et al.,* 2013; *Kwoll et al.,* 2013]. *Best and Kostaschuk* [2002] speculated that large-scale turbulence production above low-angle laboratory dunes is the result of periods of intermittent flow separation and/or strong velocity gradients in the dune leeside, while others suggest that intermittent flow separation may be too weak to cause high-magnitude turbulence production [*Roden*, 1998; *Sukhodolov et al.,* 2006]. Ultimately, the exact mechanisms responsible for macro-turbulence and suspension event generation in the absence of permanent flow separation above low-angle dunes remain unknown.

Understanding the flow structure over low-angles dunes is critical to quantify their contribution to flow resistance in natural channels. Dunes contribute to flow resistance by increasing drag exerted by the bed on the overlying flow [*Einstein and Barbarossa*, 1952; *Vanoni and Brooks*, 1957; *Engelund and Hansen*, 1967; *Van Rijn*, 1993; *Lefebvre et al.,* 2014]. Above dunes with permanent flow separation, dissipation of mean flow energy is dominated by flow separation and associated turbulence generation downstream of dune crests [*Nelson et al.,* 1993; *Nezu and Nakagawa*, 1993; *Bartholdy et al.,* 2010; *Huthoff*, 2012]. The effect of absent or intermittent flow separation on the flow resistance of low-angle dunes is not fully understood although some authors have attempted to account for it. *Ogink* [1989] and *Van Rijn* [1993] proposed an empirical reduction factor in resistance calculations originally developed for high-angle dunes. *Van Rijn* [1993] further suggested that dunes with low lee slope angles and lengths much longer than water depth do not contribute to flow resistance; consequently, many studies simply neglect low-angle dunes in resistance calculations [e.g., *Paarlberg et al.,* 2010; *Huthoff*, 2012]. For flow over sinusoidal waves, form drag has been reported to increase exponentially or quadratically with lee slope [*Henn and Sykes*, 1999; *Yoon et al.,* 2009]. Yet how form drag varies with dune lee slope remains unexplored.

Isolating the control of the dune lee slope on the flow field is essential for understanding why low-angle dunes emerge as dominant features in deep rivers and estuaries, how sediment is moved via macroturbulent structures in the absence of permanent flow separation, and how low-angle dunes contribute to flow resistance of a channel. This cannot be done with field observations at this time, and numerical models of flow over dunes require data for validation, so we explore how the lee slope angle affects flow structure and resistance experimentally. There has been some experimental work on flow over a low-angle dunes [*Ogink*, 1989; *Best and Kostaschuk*, 2002; *Sukhodolov et al.,* 2006; *Motamedi et al.,* 2012, 2014]. While useful comparisons have been drawn to flow over high-angle dunes [cf. *Best and Kostaschuk*, 2002], it is difficult to know whether differences in the flow field are due to differences in the dune lee slope angle, subtle differences in the dune morphology, bed roughness, and/or flow scaling (Reynolds number effects). In order to isolate the effect of dune lee slope angle on the flow structure and resistance, we undertook a series of experiments where we systematically varied the dune lee slopes while holding the dune morphology and flow hydraulics constant. We focus on addressing the following questions: (1) How does the dune lee slope angle affect flow separation and shear layer characteristics? (2) How is turbulence production affected by the dune lee slope angle? (3) Does the lee slope angle impact flow resistance?

2. Methods

Laboratory experiments were conducted in the River Dynamics Laboratory at Simon Fraser University in a 15 m long, 1 m wide, and 0.6 m deep glass-sided flume, equipped with a recirculating pump (capable of flows up to 0.2 $m^3 s^{-1}$) and adjustable slope (−0.5 to 2.0%).

2.1. Transport Stage Scaling

At present, no clear hydraulic scaling has been demonstrated for low- and high-angle dunes, as both dune configurations occur at the same Froude and Reynolds numbers. However, observations of natural dune morphologies and associated transport regimes indicate that low-angle dunes are more frequent in environments that are dominated by suspended bed material transport [e.g., *Smith and McLean*, 1977; *Kostaschuk and Villard*, 1996]. *Hendershot et al.* [2016] showed that dune lee slope angle covaries with suspended sediment concentrations. Therefore, we adopt a scaling where the Froude, Reynolds, and grain Reynolds numbers are lower regime, fully turbulent, and hydraulically rough, respectively, and focus on matching the transport stage between field conditions and our experiments. Transport stage (T) is defined as the ratio

Table 1. Design Experimental Flow and Dune Characteristics

Parameter	Unit	Value
Transport stage (T)	-	33
Critical Shields shear stress ($\tau_{*\,cr}$)	-	0.03
Nondimensional shear stress (τ_*)	-	1
Slope (S)	-	0.00132
Mean flow velocity (U)	(m s^{-1})	0.620
Froude Number (Fr)	-	0.443
Reynolds Number (Re)	-	1.24 E + 05
Water depth (h)	(m)	0.20
Dune height (H)	(m)	0.030
Dune length (L)	(m)	0.900
Dune aspect ratio (H/L)	-	0.0333
Dune lee slope (S_L)	(deg)	10, 20, 30

of the nondimensional shear stress (Shields number; τ_*) to its critical value for sediment entrainment ($\tau_{*\,cr}$) [*Yalin*, 1972; *Church*, 2006; *Lin and Venditti*, 2013]. The Shields number is defined as

$$\tau_* = \frac{\tau}{gD_{50}(\rho_s - \rho_w)} \quad (1)$$

where τ is the boundary shear stress, D_{50} the grain diameter, and ρ_w and ρ_s are water and sediment density, respectively. The critical value for sediment entrainment ($\tau_{*\,cr}$) varies with grain size but 0.03 is reasonable for sand-sized particles [*Brownlie*, 1981; *Van Rijn*, 1993]. In rivers, bed load-dominated conditions occur when $T < 3.3$, a mixed transport stage occurs when $3.3 < T < 33$, and a suspension-dominated condition occurs when $T > 33$ [*Dade and Friend*, 1998; *Church*, 2006; *Lin and Venditti*, 2013].

In our experiments, we adopt a Shields number of 1, which corresponds to $T = 33$ for a critical Shields number of 0.03. This is at the threshold between mixed and suspension-dominated conditions where a mobile bed experiences high suspended bed material fluxes, while remaining in the subcritical regime in which low-angle dunes occur. We then chose a flow depth (h) that could be easily accommodated with the experimental arrangements ($h = 0.2$ m) and back calculated a suitable water surface slope (S) for the experiments using the 1-D momentum balance for steady uniform flow:

$$\tau = \rho_w ghS \quad (2)$$

and $\rho_w = 1000$ kg/m^3, $\rho_s = 2650$ kg/m^3, and $D_{50} = 160$ μm. The design hydraulic parameters are summarized in Table 1. Flume slope was adjusted slightly to maintain uniform flow over the dunes, and water depth was adjusted to maintain $h = 0.2$ m. We elected to use clear water flows in our experiments to optimize conditions for laser-based velocity measurements and because we expect the macroscale structure of the flow field would only be modified at extremely high suspended sediment concentrations [e.g., *Wan and Wang*, 1994]. However, recent modeling has shown that there are some effects of particles on turbulent flow [e.g., *Marchioli et al.*, 2006; *Berzi and Jenkins*, 2008; *Schmeeckle*, 2014], suggesting this should be investigated further experimentally.

2.2. Dune Design

Three prototype dune beds were designed with lee slope angles of 10°, 20°, and 30°. Dunes were carved out of high-density styrofoam to mm-precision and coated with a thin layer (~1–1.5 D_{50}) of fine sand ($D_{50} = 160$ μm) to provide natural grain roughness. Each bed configuration consisted of 10 straight-crested dunes of one model geometry, covering a 9 m long working section of the 15 m flume.

The model dunes were designed in consideration of a collection of morphological characteristics of natural dunes in riverine and estuarine environments where dune lee slope has been measured (Elbe, Fraser, and Jamuna Rivers; Figure 1). We calculated dune dimensions using commonly cited scaling relations between flow depth and bed form dimensions [*Allen*, 1982; *Flemming*, 1988]. This resulted in dune heights and lengths of 0.03 m and 0.9 m, respectively (Table 1). Transport stage scaling relations [*Yalin*, 1972; *Lin and Venditti*, 2013] indicate that for $T = 33$, the dune aspect ratio of 0.033 is typical. The aspect ratio agrees with field observations for dunes with lee slopes of 10° and 20° (Figure 1). In order to focus our analysis on the influence of the dune lee slope angle, we chose not to change the dune aspect ratio for steeper prototype dunes. Dunes with 30° lee slopes are therefore longer relative to their heights compared to dunes in the Elbe, Fraser, and Jamuna Rivers. Nevertheless, the 30° dune dimensions are within the range of steep leeside dunes observed in rivers and estuaries (cf. data compilations in *Allen* [1982], *Flemming* [1988], and *Yalin* [1972]).

The dune shape was also selected in consideration of field observations which have shown natural dunes often exhibit a gentle rounded crest (location of highest bed elevation), sloping downward toward a sharp

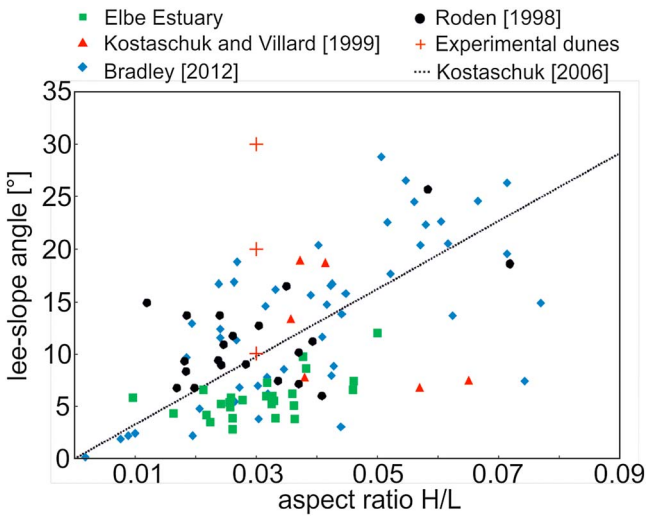

Figure 1. Dune aspect ratio (H/L) versus lee slope angle (S_L) of natural dunes from the Elbe, Fraser River [*Kostaschuk and Villard*, 1999; *Bradley*, 2012] and Jamuna River [*Roden*, 1998] and prediction based on linear relation by *Kostaschuk* [2006]. The experimental dunes of this study are indicated (red crosses).

break (brink point), and a steeper slope (lee slope) toward the dune trough [e.g., *Roden*, 1998; *Parsons et al.*, 2005; *Kostaschuk et al.*, 2009]. To approximate this phenomenon in the experiments, the dune crest is located upstream of the leeside brink point (brink point height = 0.025 m) at a distance that is equal to the horizontal extent of the leeside for all bed configurations. The resulting templates of the experimental dunes are shown in Figure 2.

2.3. Data Collection and Quality Inspection

At-a-point, high-frequency velocity measurements were obtained with a 6 W TSI Laser Doppler Velocimeter (LDV) mounted onto a robotic positioning system. The flow was seeded with 10 μm, neutrally buoyant glass particles to achieve data rates of >300 Hz. Vertical profiles composed of 60 s at-a-point time series measurements of streamwise (u) and vertical (w) velocity were measured near the flume centerline above the seventh dune to ensure that flow was fully adjusted to the dune topography. Due to the positioning system length, measurements for each set consist of two segments, between which the positioning system was physically moved. The lowest measurements were located 5–6 mm above the bed for the 20° and 30° dunes and 3 mm above the bed for the 10° dunes, as the probe was tilted. Close to the bed in the leeside and upper stoss region, data were collected with a vertical and horizontal resolution of 5 mm. Outside the leeside region, in the upper water column and on the stoss-side the resolution was reduced to 10 mm where higher spatial resolution was unnecessary (Figure 2).

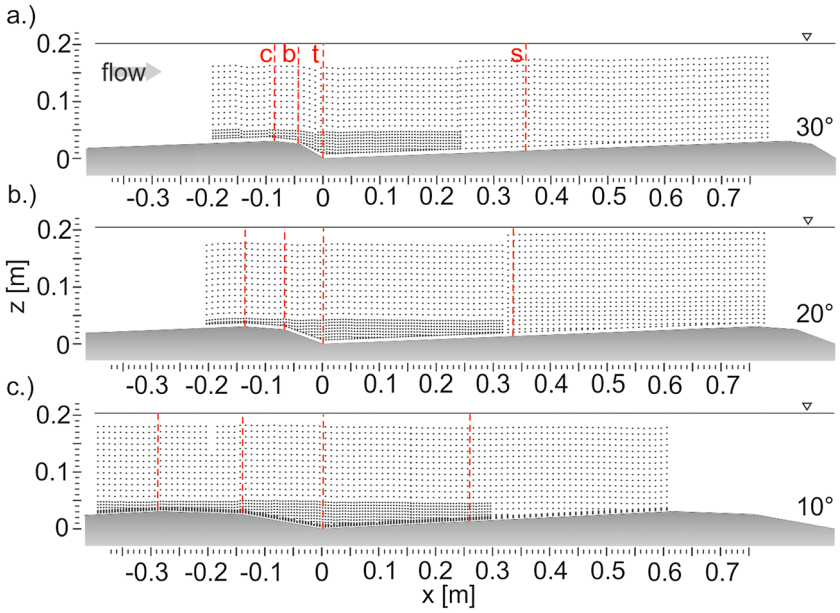

Figure 2. Experimental dune design and LDV data collection points for the three bed configurations of (a) the 30° dunes, (b) the 20°, and (c) the 10° dunes. Location of vertical profiles of Figures 4 and 7 are indicated in red (c = crest, b = brink, t = trough, and s = stoss).

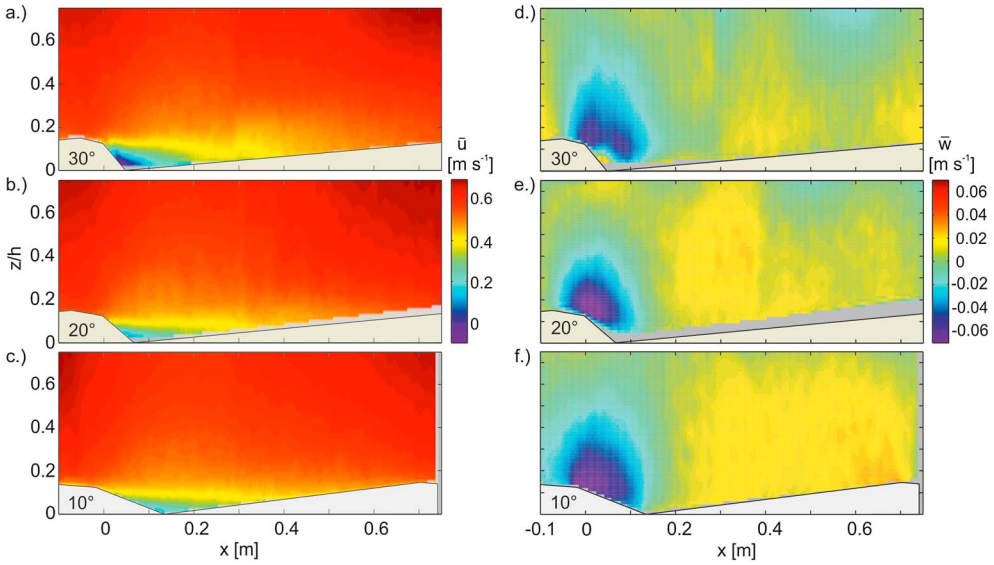

Figure 3. Mean streamwise velocity (a–c) ($\overline{u}$) (m s^{-1}) and mean vertical velocity (d–f) ($\overline{w}$) (m s^{-1}) above the 30°, 20°, and 10° dunes. Inconsistencies above the dune stoss originate from stitching of two measured segments. Flow is from left to right.

The LDV data were validated using TSI FlowSizer Software [*TSI Incorporated*, 2005] and exported for further processing. Initial quality control showed a high noise level in the vertical velocity measurements over the 10° and 20° dunes. The time series were subjected to a Gaussian low-pass filter and a despiking technique proposed by *Goring and Nikora* [2002], which reduced the noise substantially. Eventime sampling was performed by subsampling and interpolating each time series to its average data rate. Average data rates ranged from 150 to 400 Hz. Time series with data rates below 50 Hz were discarded. Velocities collected with an inclined probe were rotated about the cross-stream direction by the probe's inclination angle.

Mean flow and turbulence statistics were calculated for each time series. Results were interpolated onto a 3×3 mm grid. Some inconsistencies occurred when combining two measured segments due to probe misalignment. These inconsistencies are located above the dune midstoss (e.g., Figure 3a), at a distance downstream of the separation zone and have not been removed.

3. Mean and Turbulent Flow Field

3.1. Mean Flow Field

Time-averaged streamwise ($\overline{u}$) and vertical ($\overline{w}$) velocity components are defined as

$$\overline{u} = N^{-1} \sum_{n=1}^{N} u_i \tag{3a}$$

$$\overline{w} = N^{-1} \sum_{n=1}^{N} w_i, \tag{3b}$$

where u_i and w_i are the instantaneous velocities and N is the total number of measurements at each point. Distributions of interpolated values of $\overline{u}$ and $\overline{w}$ for all three dune geometries are shown in Figure 3. Topographic forcing of the flow by all three dune geometries is evident (Figures 3a–3c). Flow acceleration is notable above the gentle sloping dune stoss-side, and flow deceleration follows the topographical step downstream of the crest. The deceleration is more substantial downstream of the steeper dune lee slopes. Measurements of mean upstream flow are restricted to a small zone downstream of the 30° dunes (Figure 3a).

Topographic forcing is also evident in distributions of $\overline{w}$ (Figures 3d–3f), with downward directed flow in the lower half of the water column, downstream of the crest until approximately $x = 0.2$ m. Maximum downward flow is located at the brink point for all dune geometries. Above the stoss-side $\overline{w}$ is positive and increasing, denoting acceleration toward the crest. The flow field of the 30° dune (Figure 3d) has a small but distinct zone of positive vertical velocity above the immediate lower lee and trough that

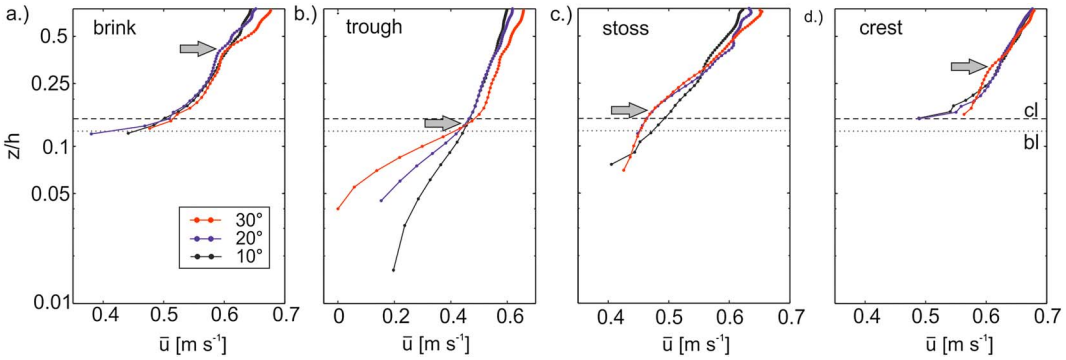

Figure 4. Vertical profiles of mean streamwise velocity ($\overline{u}$) (m s^{-1}) above selected locations along the dune profile for the three dune geometries. Horizontal black dashed and dotted lines indicate reference levels (cl = crest level, bl = brink level). Location of profiles is indicated in Figure 2. Arrows denote kinks referred to in the text.

coincides with the small zone of upstream flow (Figure 3a) indicating permanent flow reversal along the lee slope. The downward flow magnitude over the dune brink point is lowest above the 30° dunes (Figure 3d) and highest over the 20° dunes (Figure 3d). However, the zone of negative flow over the 20° dunes is smaller than over the 30° and 10° dunes (Figure 3f), suggesting that in terms of downward directed flow over the crestline, the 20° dunes represent some optimal condition in respect to the flow.

Select vertical profiles of $\overline{u}$ are shown in Figure 4 above the brink point, trough, stoss-slope, and crest. At the brink point ($x = 0$ m), vertical profiles of $\overline{u}$ (Figure 4a) near the bed ($z/h < 0.4$) are similar for all three dune geometries and are responding to grain-related drag. Above $z/h = 0.4$, $\overline{u}$ profiles are log-linear, with steeper segments and higher flow velocities occurring above the 30° dunes. Above the trough (Figure 4b), $\overline{u}$ decreases rapidly below the level of the brink point ($z/h = 0.125$), with upstream velocities occurring downstream of the 30° dunes, only (maximum -0.027 m s^{-1}). The vertical profiles are log-linear above $z/h > 0.15$ over the trough. Above the midstoss ($x = 0.45$ m), $\overline{u}$ profiles of the 30° and 20° dunes consist of two log-linear segments converging at $z/h = 0.16$ (Figure 4c). The slope of the bottom segment is higher than that of the upper segment indicating stronger flow acceleration close to the bed than higher in the water column. This segmentation occurs closer to the bed compared to the segmentation above the brink point (Figure 4a). A less pronounced kink occurs higher in the water column ($z/h = 0.3$) above the 10° dunes. At the crest (Figure 4d), $\overline{u}$ profiles of all three dune geometries are similar and log-linear in the upper water column ($z/h > 0.35$). Below, $\overline{u}$ decreases faster above the 30° dunes, while $\overline{u}$ profiles of the 10° and 20° dunes remain similar.

3.2. Flow Separation

Upstream directed time-averaged velocity is only evident downstream of the 30° dune crests indicating permanent flow separation. There may also be time-averaged upstream flow in the trough where we do not have measurements; however, if it occurred, it would be limited in extent. Our more detailed measurements at the bed over the 10° dune indicate an absence of upstream flow conclusively. Examination of the instantaneous time series however shows that intermittent flow separation occurs for all three dune geometries. Distributions of interpolated values of the intermittency factor *IF*, defined as the percentage of the measured time series at one point occupied by reversed flow [*Bennett and Best*, 1995; *Best and Kostaschuk*, 2002], are shown in Figures 5a–5c. The vertical extent of the area experiencing flow separation decreases with the dune lee slope. The intermittency factor *IF* of the 30° dunes reaches maximum values of 68.1% at the location identified as permanent flow separation in Figure 3a. The region affected by intermittent flow separation, however, has a larger extent than suggested by the time-averaged flow field. The intermittency factor *IF* decreases with height above the bed and distance downstream. Flow reversal downstream of the 20° dunes occurs for a maximum of 9.5% of the time and occupies the entire lee slope. Maximum percentage of flow reversal is 2.7% for the 10° dunes and is restricted to the dune toe. Both the number and the average duration between flow reversals increase exponentially with *IF* for all time series subject to flow reversal. Maximum flow reversal frequencies at points of highest intermittency are 12.5 Hz for the 30°, 5.3 Hz for the 20°, and 2.9 Hz for the 10° dunes.

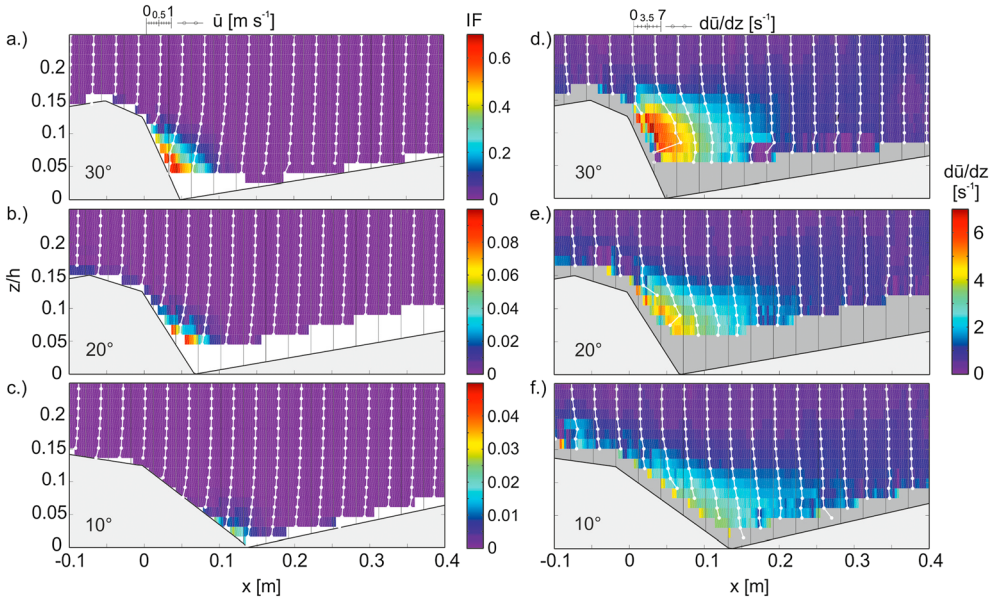

Figure 5. Intermittency factor *IF* of flow separation and vertical profiles (white) of mean streamwise velocity (a–c) $\overline{u}$ (m s^{-1}) and interpolated distributions and vertical profiles of vertical gradient of time-averaged streamwise velocity (d–f) (d$\overline{u}$/d*z*) (s^{-1}) above the (Figures 5a and 5d) 30°, (Figures 5b and 5e) 20°, and (Figures 5c and 5f) 10° dunes. Flow is from left to right. Note different color scales for *IF*.

The relation between intermittency factor *IF* and the vertical gradient of time-averaged streamwise velocity (d$\overline{u}$/d*z*) was explored by fitting a third-order polynomial to the velocity data. Downstream of the 30° dunes (Figure 5d), a region of high d$\overline{u}$/d*z* occurs downstream of the dune brink point approximately 3–4 cm above the bed. This region encloses a zone of low d$\overline{u}$/d*z* immediately above the dune lee slope that coincides with the location of maximum *IF* and permanent flow separation (Figure 5a), consistent with a free shear layer. With lower lee slope the location of strongest d$\overline{u}$/d*z* in the shear layer shifts downward away from the brink point and closer toward the bed (Figures 5e and 5f). The region of low d$\overline{u}$/d*z* adjacent to the lee slope diminishes. Downstream of the 20° (Figure 5e) and 10° dunes (Figure 5f), highest d$\overline{u}$/d*z* coincides with maximum *IF* of flow separation. Vertical profiles show a gradual increase of d$\overline{u}$/d*z* toward the bed.

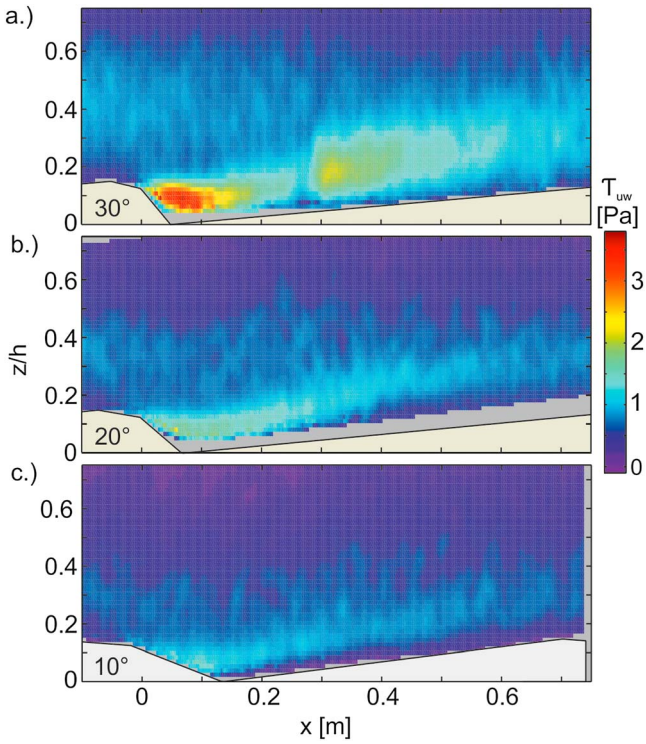

Figure 6. Principal Reynolds shear stress τ_{uw} (Pa) above the (a) 30°, (b) 20°, and (c) 10° dunes. Inconsistencies above the dune stoss originate from stitching of two measured segments. Flow is from left to right.

3.3. Turbulent Flow Field

The turbulent flow field is explored using the principal Reynolds shear stress component (τ_{uw}) calculated as

$$\tau_{uw} = -\rho_w \overline{u'w'} \qquad (4)$$

where $u' = u_i - \overline{u}$ and $w' = w_i - \overline{w}$ are the instantaneous velocity fluctuations.

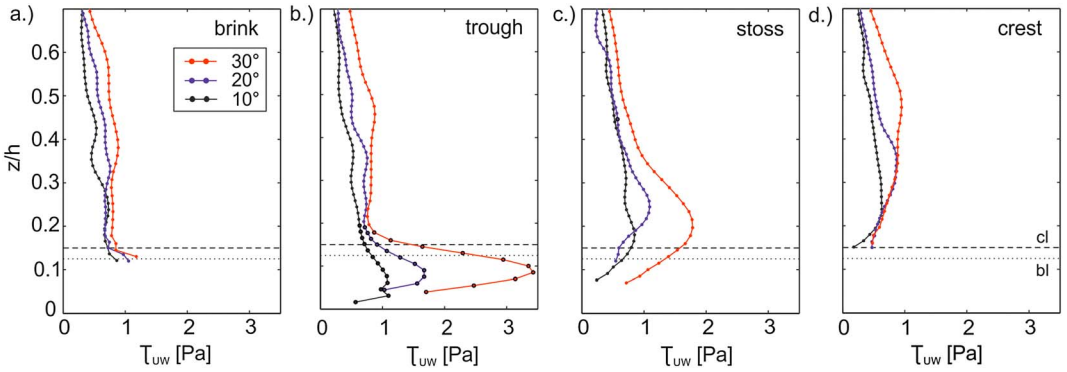

Figure 7. Vertical profiles of principal Reynolds shear stress (τ_{uw}) (Pa) at selected dune locations along the dune profile for the three dune geometries. Horizontal black dashed and dotted lines indicate reference levels (cl = crest level and bl = brink level). Location of profiles is indicated in Figure 2.

Over a flat bed, Reynolds shear stress increases linearly toward the bed. The presence of a dune alters the distributions of Reynolds stress. Previous work [*Nelson et al.*, 1993; *McLean et al.*, 1994; *Bennett and Best*, 1995; *Venditti and Bennett*, 2000; *Venditti*, 2007] has shown that maximum values of τ_{uw} typically occur at and just downstream of flow reattachment and along the shear layer.

The turbulent flow field over all three dune geometries is similar to the patterns observed in previous work (Figure 6**)**. Broadly, the greatest variability of τ_{uw} between geometries occurs in the lower water column ($z/h < 0.4$). A zone of increased τ_{uw} originates at the brink point, stretching along the stoss of the upstream dune. In this zone, τ_{uw} decreases with distance downstream, delineating the wake structure. Maximum τ_{uw} in the wake occurs over the 30° dune, and the wake structure weakens with lower lee slopes. Figure 7 directly compares vertical profiles of τ_{uw} above the three dune geometries over the dune brink point, trough, stoss-slope, and crest. Over the brink, τ_{uw} increases with lee slope angle in the upper portion of the flow (Figure 7a), and there is a distinct bulge in the upper water column for the 20° and 30° dunes, likely due to the influence of upstream wakes. Above the trough, maximum τ_{uw} increases with lee slope angle (Figure 7b). Above the midstoss, as the wake structure diffuses outward with distance away from the brink point, τ_{uw} decreases; maximum τ_{uw} however consistently occurs above the 30° dunes (Figure 7c). The linear decrease in Reynolds stress that is typically observed over flat beds occurs above the crest of all three dune geometries. However, the linear portion of the profile is confined to $z/h > 0.5$ for the 30°, to $z/h > 0.4$ over the 20° dune, and $z/h > 0.25$ over the 10° dune. This suggests that flow over the crest of the progressively lower angle dunes becomes more like flow over a flat bed.

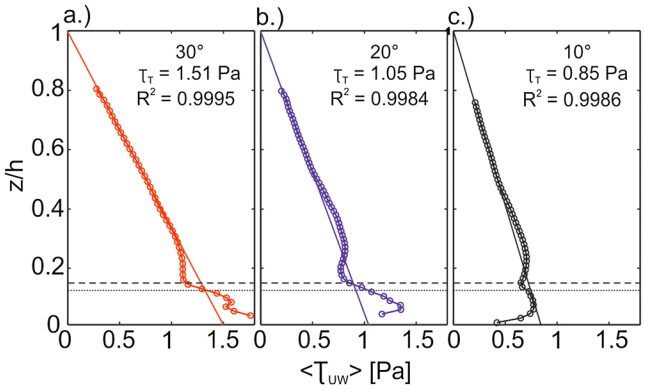

Figure 8. Double-averaged Reynolds shear stress profile $<\tau_{uw}>$ (Pa) and linear regression for determination of total shear stress τ_T (Pa) for (a) 30°, (b) 20°, and (c) 10° dunes. Coefficients of determination R^2 of linear regressions are indicated, and statistical errors are provided in Table 2.

Turbulent flow over the three dune geometries is further examined by comparing double-averaged Reynolds stress profiles. Double averaging was performed by averaging τ_{uw} in the streamwise direction over horizontal planes parallel to the mean bed elevation over one dune length [e.g., *Nikora et al.*, 2001; *McLean et al.*, 2008] and is denoted as $<\tau_{uw}>$. Double-averaged Reynolds stress profiles are shown in Figure 8. The profiles increase linearly from the water surface, form a small bulge above the level of the brink point, and reach maximum values below the brink point ($z/h = 0.125$). The linear portion is confined to $z/h > 0.3$ for the 30° dunes and $z/h > 0.5$ for the 20° and

Table 2. Total Shear Stress (τ_T), Shear Velocity (u_*), and Drag Coefficient (c_D) for the Three Dune Geometries

Lee Slope Angle S_L (deg)	Total Shear Stress τ_T[a] (Pa)	Shear Velocity u_*[a] (m s^{-1})	Drag Coefficient c_D[a]
10	0.85 ± 0.026	0.029 ± 0.00045	0.0022 ± 0.000069
20	1.05 ± 0.048	0.032 ± 0.00073	0.0027 ± 0.00012
30	1.51 ± 0.054	0.039 ± 0.00069	0.0039 ± 0.00014

[a]Statistical error calculated following *Wilkinson* [1984].

10° dunes. The secondary bulge forming above the dune brink points is least pronounced in $<\tau_{uw}>$ profiles of the 30° dunes, indicating a smaller influence of upstream wakes on the average stress profile compared to the 20° and 10° dunes. Double-averaged Reynolds stress $<\tau_{uw}>$ below the brink point for the 30° and 20° dunes is larger than the total shear stress τ_T derived from extrapolating the linear regression through $<\tau_{uw}>$ in the outer layer toward the bed [*Lyn*, 1993; *McLean et al.,* 1999]. For the 10° dunes, $<\tau_{uw}>$ below the brink point level is smaller than τ_T. The total shear stress τ_T decreases for lower lee slopes with $\tau_T = 1.51$ Pa, $\tau_T = 1.05$ Pa, and $\tau_T = 0.85$ Pa for the 30°, 20°, and 10° dunes, respectively. The shear velocity u_* and drag coefficient c_D were calculated as

$$u_* \equiv \sqrt{\tau_T \rho_w^{-1}} \tag{5}$$

$$c_D = \left(u_* U^{-1}\right)^2 \tag{6}$$

and are listed with statistical errors resulting from the least squares regression between $<\tau_{uw}>$ and z, and using a confidence limit of 97.5% [*Wilkinson*, 1984, Table 2].

3.4. Turbulence Production and Advection

Turbulent kinetic energy (TKE) is the energy extracted from the mean flow by the motion of turbulent eddies [*Kline et al.,* 1967; *Bradshaw*, 1971], and its production involves interactions of the Reynolds stresses with mean velocity gradients. Dissipation of TKE occurs by viscous forces after being passed through the inertial subrange of the turbulence spectrum [*Tennekes and Lumley*, 1972]. Over a flat bed, TKE is largest near the boundary where turbulence production is highest [*Kline et al.,* 1967]. Over a dune, elevated TKE values occur in the separation zone, at the reattachment point, and along the wake structure [*Venditti and Bennett*, 2000; *Venditti*, 2007].

The turbulent kinetic energy per unit volume written in two dimensions (streamwise and vertical; TKE_{uw}) is calculated as

$$\mathrm{TKE}_{uw} = {}^1\!/_2\, \rho_w \left(\overline{u'^2} + \overline{w'^2}\right). \tag{7}$$

Distributions of interpolated values TKE_{uw} depict near-bed wake structures with high TKE_{uw} downstream of all three dune geometries (Figures 9a–9c). Highest TKE_{uw} occurs in the immediate lee and wake of the 30° dunes (Figure 9a). TKE_{uw} is lower downstream of the 10° and 20° dunes. No secondary maximum in TKE_{uw} is observed close to the bed at flow reattachment.

Turbulence production (P) is calculated as

$$P = -\overline{u'w'}\,\frac{d\bar{u}}{dz}. \tag{8}$$

Turbulence production (P) is highest in the leeside and trough region for all three dune geometries (Figures 9d–9f), indicating that the dominant source of turbulence is intermittent flow separation. Largest P occurs in the lee of the 30° dunes, and a local maximum (0.021 m^2 s^{-3}) occurs close to the brink point, above the upper lee slope (Figure 9d). This region coincides with highest velocity gradients associated with the free shear layer that extents from the brink point toward the bed (Figure 5d). Turbulence production below this zone of maximum productivity decreases toward the bed, with low production in the region of reversed flow adjacent the lee slope. Turbulence production in the lee of the 20° dunes is approximately half of that above the 30° dunes, with maximum production (0.011 m^2 s^{-3}) occurring at a location lower on the lee slope.

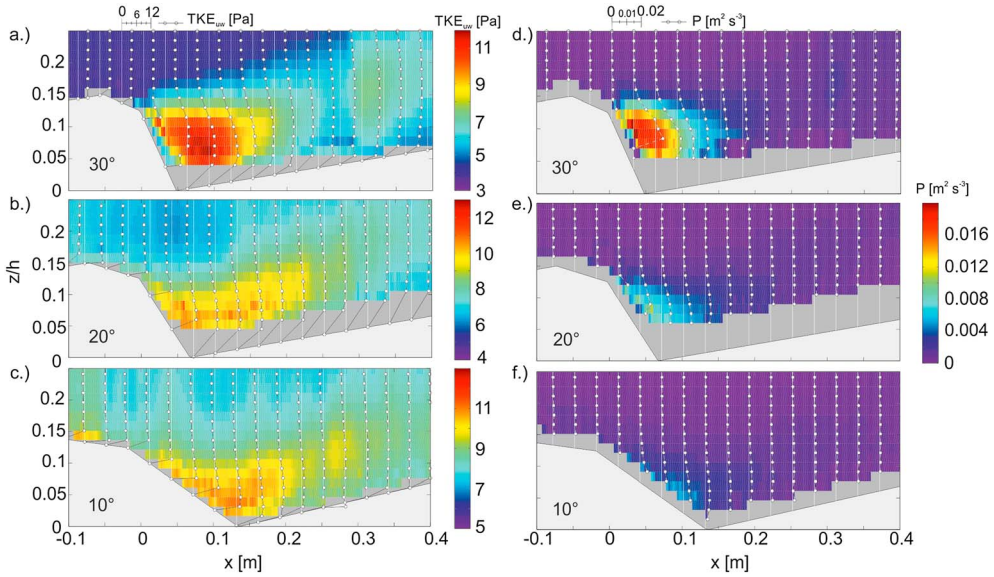

Figure 9. Turbulent kinetic energy (a–c) (TKE$_{uw}$) (Pa) and turbulence production (d–f) (P) (m^2 s^{-3}) and downstream of the brink point for the (Figures 9a and 9d) 30°, (Figures 9b and 9e) 20°, and (Figures 9c and 9f) 10° dunes. Flow is from left to right. Note different color scales for TKE$_{uw}$.

Downstream of the 10° dunes, the region of high turbulence production approaches the bed at the toe of the dune (maximum 0.006 m^2 s^{-3}). Regions of low turbulence production, as observed adjacent the lee slope of the 30° dunes, are not detected over the 10° and 20° dunes.

3.5. Characteristics of Turbulent Events

Turbulent events are examined using quadrant analysis [e.g., *Lu and Willmarth*, 1973; *Antonia*, 1981; *Nezu and Nakagawa*, 1993] where pairs of streamwise and vertical velocity fluctuations are grouped into the four quadrants spanning the u'-w'-plane. Velocity measurements are classified as outward interaction (Q1: $u' > 0$ and $w' > 0$), ejection (Q2: $u' < 0$ and $w' > 0$), inward interaction (Q3: $u' < 0$ and $w' < 0$), or sweep (Q4: $u' > 0$ and $w' < 0$). Ejections and sweeps contribute positively to Reynolds stress and therefore denote turbulence production, while outward and inward interactions contribute negatively and indicate energy transfer to the mean flow field. A holesize (HS) is traditionally applied [*Lu and Willmarth*, 1973; *Bennett and Best*, 1995; *Best and Kostaschuk*, 2002] to differentiate lower and higher magnitude $|u'w'|$ events:

$$|u'w'| > \mathrm{HS} * (u'_{\mathrm{rms}} w'_{\mathrm{rms}}) \tag{9}$$

where u'_{rms} and w'_{rms} are the root-mean-square values of velocity fluctuations.

Figure 10 shows the spatial distribution of percentages of velocity observations in each quadrant above the three types of bed forms for $HS = 2$. Previous studies have shown that a value of 2 is appropriate to separate large-scale events from background fluctuations [*Bennett and Best*, 1995; *Best and Kostaschuk*, 2002; *Yue et al.*, 2006]. The majority of observations fall into Q2 and Q4 and to a lesser degree into Q1 and Q3 for all three dune geometries. The number of observations in Q2 and Q4 above $HS = 2$ declines with lee slope, showing that larger-scale motions become rarer. Ejection events dominate the flow field, particularly in the shear layer extending from the dune crests and wake (Figure 10a). Sweeps dominate in the near-bed region below the shear layer above the stoss-side of the dunes and immediately downstream of the crest (Figure 10d). Downstream of the 30° dunes the sweep-dominated region extends along the entire stoss-side but decreases in extent with the dune lee slope. The distribution of Q1 and Q3 events (Figures 10b and 10c) mirror these patterns in that Q1 events are particularly rare along the shear layer and Q3 events particularly rare in the sweep-dominated regions.

The frequencies of turbulent events in the shear layer and in the wake are further explored by grouping consecutive observations in both Q2 and Q4 and determining the group or event frequency (Figure 11). We focus on Q2 and Q4 because they contribute to turbulence production. The frequencies of ejection and sweep

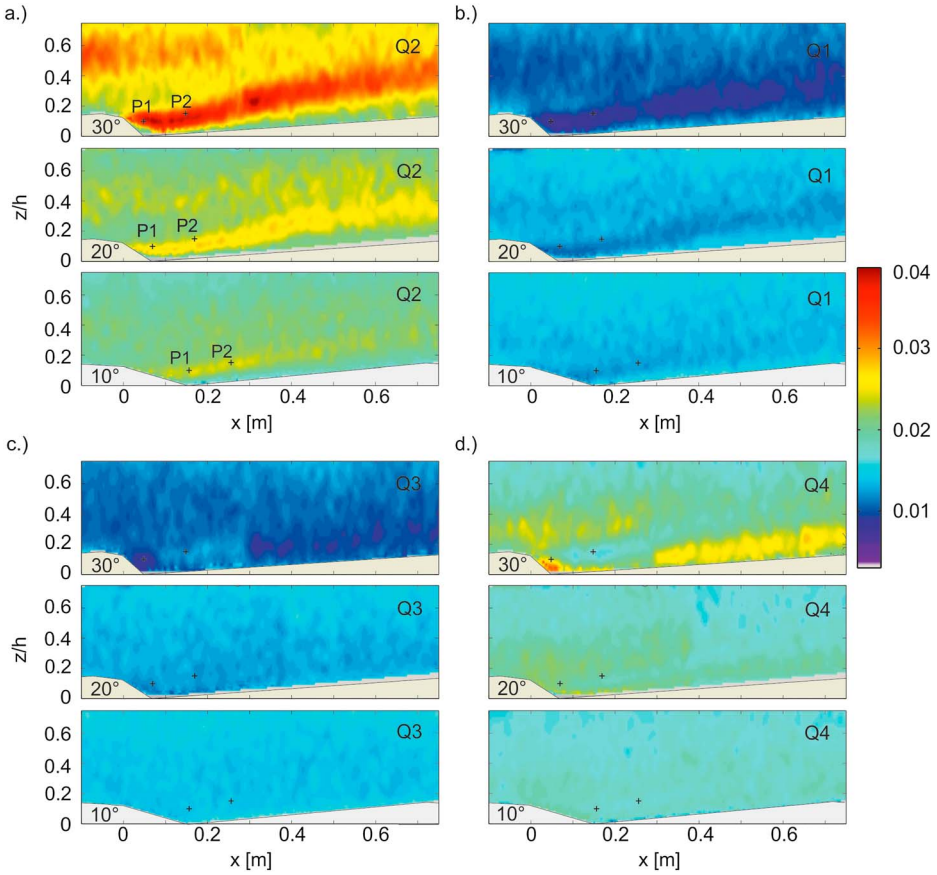

Figure 10. Spatial distribution of the percentage of observations in each quadrant above a holesize of $HS = 2$ [cf. *Lu and Willmarth*, 1973] for all three dune geometries. P1 and P2 denote locations of more detailed time series analysis in Figure 11.

events along the shear layer (P1, Figures 11a–11c) and in the wake (P2, Figures 11d–11f) decrease asymptotically with *HS* and become small for $HS > 3$. Sweeps are more frequent than ejections for small *HS*, and the opposite is true for large *HS*. This indicates that sweeps are more frequent but lower intensity than ejection events. At higher values of *HS*, the lower intensity sweeps have been removed, and the stronger ejections dominate. The difference is strongest in the shear layer of the 30° dune and less prominent in the wake and for lower angle dunes. The dependency of frequency on *HS* makes it difficult to establish the frequency of turbulent events using this method. Table 3 summarizes the frequencies for various values of *HS* and shows that the frequency of the large-scale ejection events decreases with lee slope.

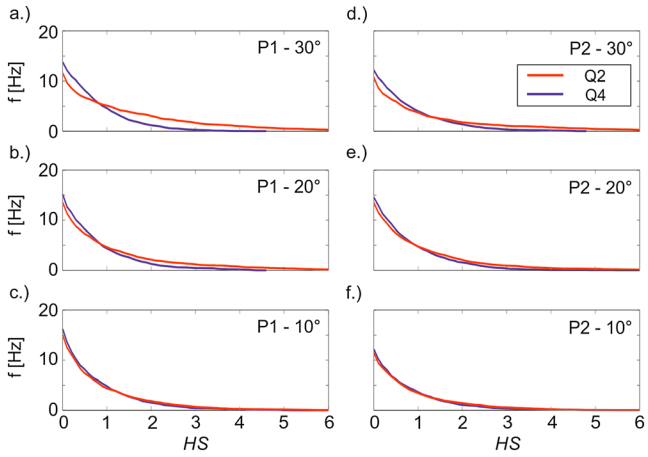

Figure 11. Frequency of groups of ejection (Q2) and sweep (Q4) events as a function of the holesize (*HS*) in the shear layer (P1) and wake (P2) indicated in Figure 10 ((a and d): 30° dunes, (b and e): 20° dunes, (c and f): 10° dunes).

We also explored the frequency of turbulent events using red noise spectral analysis techniques because turbulent velocity time series are highly autocorrelated. Time series were detrended and analyzed using the MATLAB redconf.m

Table 3. The Frequency (f) of Ejection (Q2) Events at a Location in the Shear Layer (P1) and Wake (P2) at Selected Holesizes (HS)

Location (Figure 11)	Lee Slope Angle S_L (deg)	f (Hz) $HS = 1$	$HS = 2$	$HS = 3$
P1	30	5.13	3.02	1.66
	20	4.65	2.15	1.21
	10	4.39	1.86	0.69
P2	30	3.74	1.77	1.08
	20	4.76	2.08	0.95
	10	3.43	1.43	0.58

program [*Husson*, 2012] which calculates spectral power density using the Thomson multitaper approach [*Thomson*, 1982], tests the amount of red noise in the data, and computes the confidence limits. Spectra in the shear layer and in the wake showed high coincidence with a red noise turbulence spectrum with a $-5/3$ slope spectral roll off at frequencies > 1 Hz. A statistically significant low frequency peak emerges at 0.1–0.3 Hz in some of the spectra, corresponding to 1–3 events per 10 s. There are no other statistically significant peaks in the spectra at higher frequencies. This suggests that higher-frequency turbulent events in these regions are aperiodic and randomly generated events.

4. Discussion

4.1. How Does the Dune Lee Slope Angle Affect Flow Separation and Shear Layer Characteristics?

Simpson [1989] classified flow separation as incipient (<1% of the time), intermittent (1–20% of the time), transitory (20–50% of the time), and permanent (≥50% of the time) when the time-averaged bed shear stress is zero, meaning that upstream and downstream fluctuations in velocity balance to produce negligible shear stresses. Observations of flow separation over dunes produce a wide variety of results. Based on collections of previous flow measurements, several authors suggested that permanent flow separation occurs for lee slopes > 10° [e.g., *Wilbers*, 2004; *Paarlberg et al.,* 2009]. Field observations suggest that flow separation is absent [e.g., *Smith and McLean*, 1977; *Kostaschuk and Villard*, 1996; *Parsons et al.,* 2005; *Bradley et al.,* 2013] or intermittent [*Roden*, 1998; *Carling et al.,* 2000a] for dunes with lee slopes up to 19°. However, it is difficult to measure flow reversal over dunes in the field, and therefore, it is not clear whether this empirically derived limit is real.

Laboratory measurements can provide clearer results because it is possible to take reliable measurements in the lee of dunes. However, previous observations of flow over low-angle dunes are too limited to narrow down the critical lee slope for permanent and intermittent flow separation. Most studies simply report the presence or absence of permanent or intermittent flow separation [cf. *Best and Kostaschuk*, 2002; *Sukhodolov et al.,* 2006; *Motamedi et al.,* 2012, 2014]. Direct comparison of these results is problematic because the occurrence of flow separation is known to be dependent on roughness [*Britter et al.,* 1981; *Wood*, 1995; *Gong et al.,* 1996; *Cao and Tamura*, 2006; *Lefebvre et al.,* 2014] and Reynolds number [*Zilker and Hanratty*, 1979].

Studies of air flow over sinusoidal waves with Reynolds numbers in the rough turbulent regime provide clearer indications of when to expect permanent and intermittent flow separation. These studies suggest that permanent flow separation occurs for maximum wave lee slopes >20° [e.g., *Zilker et al.,* 1977; *Dellil et al.,* 2004; *Yoon et al.,* 2009], while intermittent separation occurs for maximum lee slopes as low as 14° [*Britter et al.,* 1981; *Gong and Ibbetson*, 1989; *Kuzan et al.,* 1989; *Yoon et al.,* 2009]. Work on flow over negative steps suggests that the critical lee slope for permanent flow separation is 15° [*Ruck and Makiola*, 1990]. There is also some evidence of intermittent flow separation in conical diffusers, which would be equivalent to a 4° lee slope [*Azad*, 1996] (see discussion in *Best and Kostaschuk* [2002]).

Here we systematically isolated the effect of the dune lee slope while holding surface roughness, Reynolds number, and other bed form geometry and hydraulic parameters constant. This permits direct comparison of the flow fields, which has not been previously possible. Permanent flow separation ($IF \geq 50\%$) only occurs downstream of our 30° dunes ($IF = 68.1\%$), which we could reasonably predict from previous work on flow over dunes, negative steps, and sinusoidal waves. However, the observation of intermittent flow separation over the 20° ($IF = 9.4\%$) and 10° dunes ($IF = 2.7\%$) is surprising. Based on flow over sinusoidal waves, we would predict the 20° dune to be close to the threshold for intermittent to permanent separation, which it is not. We would not expect any separation over the 10° dune. Using previous observations over a negative step, we would predict the 20° dune to exhibit permanent flow separation, which it does not. This suggests that

drawing direct comparisons between flow separation over low-angle dunes and similar topographies (negative steps and sinusoidal waves) is problematic. Our detailed maps of flow intermittency also suggest that whether flow separation is detected is strongly dependent on where measurements are taken, as regions affected by weaker flow reversal decrease in size with lower lee slope toward the toe of the dune. Individual measurements in the lee of a low-angle dune may or may not reveal intermittent flow separation depending on where the observation is made. The highest intermittency values occur closest to the bed, which given the challenges of high-resolution measurements near the bed, may explain the variations in reported separation in the field and laboratory.

A further potentially influencing factor for observing the occurrence and degree of intermittency of flow separation is the angle of the slope leading from the crest to the brink point. For sinusoidal waves the gentle slope leading from the crest toward the maximum lee slope will increase with increasing maximum lee slope; a feature simulated with our experimental dunes in that the angle leading down to the brink point increases from 2° to 6.6° from the 10° to the 30° dunes. Therefore, flow approaching the brink point encounters a weak adverse pressure gradient, and deceleration before the maximum slope is encountered. This will cause a lower pressure differential downstream of the brink point, which may influence flow separation. *Paarlberg et al.* [2007] note a dependence of the dip of the separation streamline on the bed-slope at the brink point, resulting in smaller separation zones for higher, downward slopes at the point of separation. This may explain why permanent flow separation is observed over a sharp-crested negative step at 15^{o} [*Ruck and Makiola*, 1993] and not over more gentle-crested sinusoidal waves and dunes. Nonetheless, the small gradient between the crest and brink point occurs over a natural dune, so we suspect the effects on separation are apt to also translate well from our model to natural dunes.

There is an explicit linkage between the degree of intermittency of flow separation and velocity gradients [*Roden*, 1998; *Best and Kostaschuk*, 2002]. In our experiments, we observe high velocity gradients in the lee-side of all three dune geometries with the maximum gradient occurring immediately below the brink point on the upper lee slope. The shear layer is detached from the bed downstream of the 30° dunes and occurs closer to the bed for less steep lee slopes. The magnitude of the velocity gradient within the shear layer decreases with lee slope angle. Velocity gradients inside the shear layer for all our dune geometries, however, are higher than velocity gradients in the near-bed region of attached flow associated with the redevelopment of the IBL. Maximum gradients downstream of the 20° and 10° dunes are 70% and 55% of maximum gradients downstream of the 30° dunes, respectively. *Ruck and Makiola* [1993] attributed a reduction in velocity gradients for lower inclination angles of a negative step to a damping of shear layer expansion by the increasing proximity between shear layer and wall, consistent with our observations.

4.2. How Is Turbulence Production Affected by the Dune Lee Slope Angle?

The production of turbulence over a flat bed is dominated by structures originating at the boundary that dissipate, as they move vertically. Over high-angle dunes, production is concentrated along the free shear layer associated with flow separation and within the zone of separated flow [*Nelson et al.,* 1993; *Venditti and Bennett*, 2000]. This zone of turbulence production produces the wake structure that is diffused downstream. Turbulence production and wake formation associated with low-angle dunes have often been assumed negligible [e.g., *Huthoff*, 2012] despite observations of macroturbulent structures carrying large volumes of sediment in suspension [*Kostaschuk and Church*, 1993; *Kostaschuk and Villard*, 1999; *Bradley et al.,* 2013; *Kwoll et al.,* 2014]. Laboratory experiments, however, have previously documented wake structure formation downstream of low-angle dunes [*Best and Kostaschuk,* 2002; *Sukhodolov et al.,* 2006] and negative steps with low step angle [*Ruck and Makiola*, 1990], indicating a contrast to turbulence production over a flat bed.

Our measurements above the 30° dunes show high turbulence production along a free shear layer and a wake structure, revealed by high Reynolds stresses and TKE, consistent with previous observations [e.g., *Nelson et al.,* 1993; *Venditti and Bennett*, 2000]. Maximum TKE is located at approximately half the brink point height at flow reattachment and thus higher in the flow than measurements of *Venditti and Bennett* [2000]. Downstream of the 20° and 10° dunes, a wake structure extends from the brink point with lower magnitude Reynolds stresses and TKE compared to the 30° dune geometry. The onset of the wake structure and region of highest turbulence production occurs closer to the lee slope compared to the 30° dune case, agreeing with observations by *Best and Kostaschuk* [2002] and *Yoon et al.* [2009]. Our results enable us to link this transition

of high turbulence toward the lee slope to the vertical position of the shear layer. Further, our systematic analysis demonstrates that the decrease in turbulence production and strength of the wake is nonlinear with a significantly higher reduction in wake strength between the 30° and 20° dunes than between the 20° and 10° dunes.

In the presence of permanent flow separation, turbulence production is thought to take the form of large-scale flow structures shed from Kelvin-Helmholtz type instabilities along the free shear layer [e.g., *Müller and Gyr*, 1986; *Simpson*, 1996; *Kadota and Nezu*, 1999]. Shear layer expansion with distance downstream is thought to encourage growth of these instabilities until they begin diffusing in the wake. *Best and Kostaschuk* [2002] speculated that large-scale turbulence production above low-angle dunes similarly occurs due to eddy shedding in temporary regions of high velocity gradients during intermittent flow reversal and/or interaction of flow deceleration in the dune lee with the flow field of upstream dunes. They further hypothesize that large-scale structures are smaller and occur less frequently compared to structures originating from the free shear layer associated with permanent flow separation. It has also been speculated that large-scale turbulent production is absent above low-angle dunes [*Sukhodolov et al.,* 2006].

Our measurements show that a shear layer emerges with or without permanent flow separation and that the shear layer is intrinsically linked to turbulence production downstream of low-angle dunes. We show that spread of the shear layer is damped for lower lee slopes due to the proximity of the bed, which could affect eddy shedding processes in the lee of the low-angle dunes. Our quadrant analysis shows a decrease in frequency of large-scale events along the shear layer and in the wake (identifiable as strong ejections) with lee slope. This supports *Best and Kostaschuk* [2002] speculation that lower frequency and magnitude events dominate along the shear layer of low-angle dunes. The spatial maps seem to reject the idea that the large scale events are produced by boundary layer bursting. However, further work is necessary to better understand the typology of the ejection events that we document along the shear layer and in the wake structure. This can only be accomplished by spatially and time-resolved measurements, as the structures develop in the dune lee for of low- and high-angle dunes.

4.3. Does the Lee Slope Angle Impact Flow Resistance?

The quantification of dune-related flow resistance constitutes a major challenge in hydraulic and morphodynamic modeling of river and coastal evolution [*Paarlberg et al.,* 2010; *Warmink et al.,* 2013; *Winter et al.,* 2006]. Several approaches have emerged to relate measurable parameters of dune morphology to quantifiable measures of flow resistance. The simplest relations are based on dune length and height and stem from empirical assessment of flow field measurements above dunes [e.g., *Nelson and Smith*, 1989; *Van Rijn*, 1993]. *Ogink* [1989] and *Van Rijn* [1993] observed overestimation of dune-related flow resistance for lee slopes below the angle-of-repose and proposed using an empirical reduction factor. Other studies have assumed that flow resistance exerted by low-angle dunes is negligible [e.g., *Paarlberg et al.,* 2009; *Huthoff*, 2012].

The dominant factor controlling flow resistance of dunes is the energy expenditure associated with flow separation [*Nelson et al.,* 1993; *Nezu and Nakagawa*, 1993; *Bartholdy et al.,* 2010; *Huthoff*, 2012; *Lefebvre et al.,* 2014]. There are several methods that have been proposed to predict the spatial extent of flow separation [*Wilbers*, 2004; *Paarlberg et al.,* 2007, 2010]. *Wilbers* [2004] suggested that the zero-velocity-line inside the flow separation region slopes from the brink point toward flow reattachment with an approximate angle of 10°. Below this zero-velocity line, flow will tend to move upstream, downstream of the zero-velocity line flow reattaches, and follows the stoss of the downstream dune. Using a third-order polynomial function, *Paarlberg et al.* [2007] developed a parameterization of the shape of the separation streamline bordering the region affected by flow separation downstream of dunes. The separation streamline is defined as the line below which the integral of streamwise velocity is zero. Separation streamline and reattachment are calculated based on dune height and angle of slope leading to the brink point (see *Paarlberg et al.* [2007] for detailed derivation).

Figure 12 shows a metric of flow separation as the product of the intermittency factor and the maximum observed upstream flow ($IF \times -u_{max}$) and the predicted extent of flow separation for our dune morphologies. Higher values of $IF \times -u_{max}$ indicate more frequent and stronger upstream flow. Low values of $IF \times -u_{max}$ suggest the absence of flow separation. The extent of flow separation over all three dune shapes is relatively well defined, although the absence of data near the boundary over the 20° dune leaves some uncertainty in this regard. Over the high-angle dune (30°), flow separates at the brink point, while over the lower angle

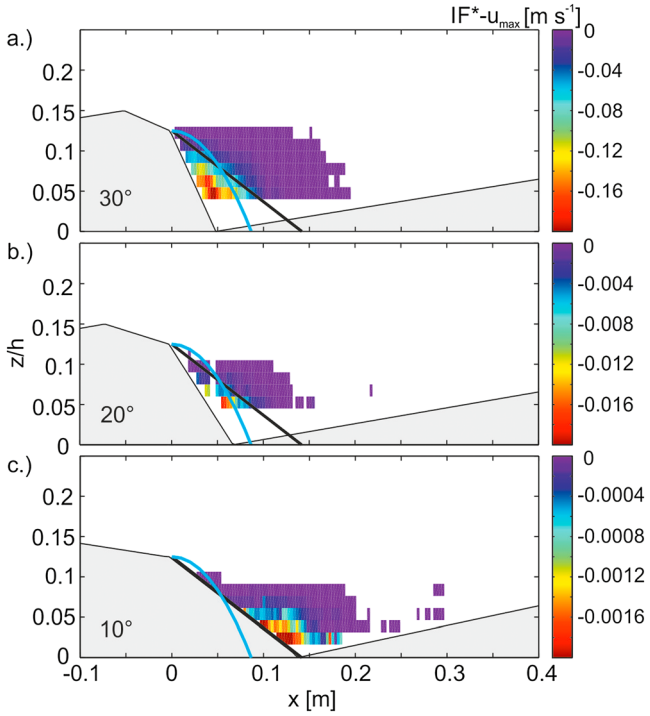

Figure 12. Intermittency factor (*IF*) *Maximum upstream flow ($-u_{max}$) (m s^{-1}) and predictions of the zero-velocity-line (black) of *Wilbers* [2004] and separation streamline (blue) of *Paarlberg et al.* [2007] downstream of the (a) 30°, (b) 20°, and (c) 10° dunes. Note different color scales.

dunes, intermittent separation appears to occur lower down on the stoss-slope (Figure 12). Methods to predict the flow separation region geometry are consistent with the patterns of high $IF \times -u_{max}$ over the high-angle (30°) dune; however, the length of intermittent flow separation is much longer than would be predicted (Figure 12a). Perhaps not surprisingly, the model predictions over the 10° and 20° dunes are of limited value because the methods do not account for intermittent separation and the separation point no longer coincides with the brink point.

An alternative approach to quantifying the effect of the lee slope angle on flow resistance is to compare the calculated shear stresses to the stress associated with a flat bed. This was done using the depth-averaged version of the law of the wall:

$$\frac{U}{u_{*_s}} = \frac{1}{\kappa} ln\left(11\frac{h}{k_s}\right) \quad (10)$$

where κ is the von Karman constant (0.4), u_{*s} is the shear velocity that would occur in the absence of form roughness in the channel, and $k_s = 2\,D_{50}$ is the sand roughness applied to the bed [*van Rijn*, 1993]. The shear stress ($\tau_s = \rho u_{*s}^2$) associated with a flat bed at the same discharge, velocity, and depth is 0.79 Pa. Figure 13 shows the increase in the ratio τ_T/τ_s, as the dune lee slope angle increases from 0 (flat bed) to 30°. The increase in τ_T/τ_s is reasonably well approximated by

$$\frac{\tau_T}{\tau_s} = 1 + 0.001 S_L^2 \quad (11)$$

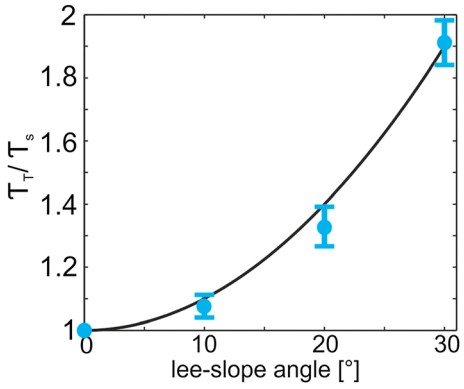

Figure 13. Ratio of the shear stress associated with a flat bed at the same discharge, velocity, and depth without bed forms and the measured shear stress [τ_T/τ_S] with error bars derived from regression analysis [*Wilkinson*, 1984] for each lee slope angle. Black line indicates the approximation of equation (11).

where S_L is the lee slope angle. The 30° dune approximately doubles the shear stress ($\tau_T = 1.9\tau_s$). Reducing the lee slope angle reduces the temporal occurrence of flow separation and the flow resistance. Shear stress over the 20° and 10° dunes are ~33% and 8% greater than a flat bed, respectively. This is a 70% and 56% reduction in shear stress over the 20° and 10° dunes, compared to a 30° dune. Our results show that low-angle dunes contribute a lesser but still substantial amount of flow resistance. Neglecting this effect in natural settings will lead to underestimations of total flow resistance.

Using our results (Figure 13 and equation (11)) as a universal adjustment to dune flow resistance coefficients should be done with some caution. Our reductions in shear stress are accurate for the dune shapes we tested. Dunes with different shapes (e.g., more or less symmetrical) than ours may have different effects on the intermittency of flow separation and thus the form of equation (11).

One way to test the universality of equation (11) is to explore reductions in shear stress with changes in dune lee slope angle using numerical modeling. High-resolution, turbulence-resolving large eddy simulations and hybrids are increasingly applied to turbulent flow over dunes [e.g., *Stoesser et al.,* 2008; *Omidyeganeh and Piomelli*, 2011; *Chang and Constantinescu*, 2013; *Schmeeckle*, 2014]. That level of sophistication is required to resolve the topology of unsteady flow structures but may not be required to examine hydraulic roughness. A 2-D Reynolds-averaged Navier-Stokes (RANS) model with a k-ε turbulence closure [e.g., *Lefebvre et al.,* 2013, 2014], using our data for calibration and validation, may be better suited to roughness calculations. Such a model could be used to develop a family of curves similar to equation (11) for adjusting flow resistance coefficients for different dune shapes and lee slope angles. While a RANS model cannot reproduce the intermittency of the separation region that we document, other metrics such as the turbulent properties of the wake can be used as a metric to estimate flow resistance of low-angle dunes [cf. *Lefebvre et al.,* 2014].

5. Conclusions

We examined effects of dune lee slope on flow separation and flow resistance by measuring the flow field for lee slopes of 30°, 20°, and 10°, thereby contrasting dunes of high ($\geq$30°) and low-angle lee slopes ($<$30°), while holding other dune geometric parameters and channel hydraulics constant. The data suggest the following conclusions:

1. The temporal occurrence, magnitude, and extent of flow reversal decrease with the lee slope angle but may be fully absent downstream of dunes with lee slopes $<<$10° only. The smaller extent of intermittent separation downstream of low-angle dunes is shifted toward the dune toe rendering its detection particularly difficult in the field and laboratory.
2. A shear layer of high velocity gradients exists downstream of the brink point of high- and low-angle dunes. For low-angle dunes, this layer occurs in close proximity to the bed, and velocity gradients are reduced compared to velocity gradients of a free shear layer downstream of high-angle dunes.
3. Turbulence production is concentrated in the leeside region along this shear layer and induces a momentum loss and high turbulence intensities that are advected in a wake structure. The strength of the wake decreases nonlinearly for lower lee slopes, but the wake persists. Lower turbulence production downstream of low-angle dunes is attributed to lower velocity gradients inside the shear layer and damping of turbulence by the proximity of the bed.
4. Strong ejection events dominate the shear layer and wake region. The frequency of events decreases asymptotically with magnitude threshold (holesize). The near-bed region on the stoss-side of high-angle dunes is dominated by sweep events. This region diminishes for low-angle dunes. This suggests that sweeps may play a less important role in sediment transport over low-angle dunes.
5. Flow resistance decreases with the dune lee slope. This is in relation to the decrease in turbulence production and therefore energy expenditure downstream of dunes with lower lee slopes. Estimates of hydraulic roughness based on dune height will overpredict hydraulic roughness and may reduce the accuracy of water level predictions of hydraulic and morphodynamic models. Flow resistance of low-angle dunes, however, is not negligible, as turbulence is produced by intermittent flow separation.
6. The increase in shear stress and flow resistance with lee slope angle is nonlinear, reflecting nonlinear variation in the turbulent flow field. This implies that small changes in the lee slope for steep dunes may induce large variations in turbulence production, wake structure characteristics, and flow resistance, while equivalent changes in slope for less steep dunes may have a smaller effect.

The final conclusion has important implications for dunes in unsteady flow conditions such as occur in tidal settings or during floods, as dunes adapt their shape on timescales from minutes to hours to days, as transport stage changes. The nonlinearity in flow resistance with changing dune shape, which is known to be linked to changes in transport stage, begs for a more complete understanding for why low-angle dunes form. Future work needs to explore the time-dependent flow field in the dune lee region. Particular attention needs to be paid to temporal changes in the shear layer, the intermittent separation region, and the development of larger-scale coherent flow structures over low-angle dunes.

Acknowledgments

This research was funded through the DFG-Research Center/Cluster of Excellence "The Ocean in the Earth System". Travel grants to E.K. were provided by the Central Research Development Fund of the University of Bremen and the Bremen International Graduate School for Marine Sciences (GLOMAR). The experimental work was supported by grants to J.V. from the Canadian Foundation for Innovation, Leaders Opportunity Fund, and a NSERC Discovery Grant. Supplementary data are available through the Publishing Network PANGEA at doi:10.1594/PANGAEA.858186.

References

Allen, J. R. L. (1982), *Sedimentary Structures, Their Character and Physical Basis*, Elsevier Sci., New York.

Amsler, M., and M. Schreider (1999), Dunes height prediction at floods in the Parana River, Argentina, in *River Sedimentation*, edited by A. W. Jayawardena, J. H. W. Lee, and Z. Y. Wang, pp. 615–620, Balkema, Rotterdam.

Antonia, R. A. (1981), Conditional sampling in turbulence measurements, *Annu. Rev. Fluid Mech.*, *12*, 131–156.
Azad, R. S. (1996), Turbulent flow in conical diffuser: A review, *Exp. Therm. Fluid Sci.*, *13*(4), 318–337.
Bartholdy, J., B. W. Flemming, V. B. Ernstsen, and C. Winter (2010), Hydraulic roughness over simple subaqueous dunes, *Geo-Mar. Lett.*, *30*(1), 63–76.
Bennett, S. J., and J. L. Best (1995), Mean flow and turbulence structure over fixed, two-dimensional dunes: Implications for sediment transport and bedform stability, *Sedimentology*, *42*(3), 491–513, doi:10.1111/j.1365-3091.1995.tb00386.x.
Berzi, D., and J. T. Jenkins (2008), A theoretical analysis of free-surface flows of saturated granular-liquid mixtures, *J. Fluid Mech.*, *608*, 393–410, doi:10.1017/S0022112008002401.
Best, J. (1996), The fluid dynamics of small-scale alluvial bedforms, in *Advances in Fluvial Dynamics and Stratigraphy*, edited by P. Carling and M. Dawson, pp. 67–125, Wiley, Chichester.
Best, J. (2005), The fluid dynamics of river dunes: A review and some future research directions, *J. Geophys. Res.*, *110*, F04S02, doi:10.1029/2004JF000218.
Best, J., and R. A. Kostaschuk (2002), An experimental study of turbulent flow over a low-angle dune, *J. Geophys. Res.*, *107*(C9), 3135, doi:10.1029/2000JC000294.
Bradley, R. W. (2012), Coherent Flow Structures and Suspension Events over Low-angle Dunes: Fraser River, MSc thesis, Simon Fraser Univ., Burnaby.
Bradley, R. W., J. G. Venditti, R. A. Kostaschuk, M. Church, M. Hendershot, and M. A. Allison (2013), Flow and sediment suspension events over low-angle dunes: Fraser Estuary, Canada, *J. Geophys. Res. Earth Surf.*, *118*, 1693–1709, doi:10.1002/jgrf.20118.
Bradshaw, P. (1971), *An Introduction to Turbulence and its Measurement*, *Thermodyn.*, edited by W. A. Woods, Pergamon, Oxford.
Bridge, J. S., and J. L. Best (1988), Flow, sediment transport and bedform dynamics over the transition from dunes to upper-stage plane beds: Implications for the formation of planar laminae, *Sedimentology*, *35*(5), 753–763.
Britter, R. E., J. C. R. Hunt, and K. J. Richards (1981), Air flow over a two-dimensional hill: Studies of velocity speed-up, roughness effects and turbulence, *Q. J. R. Meteorol. Soc.*, *107*(451), 91–110.
Brownlie, W. R. (1981), *Prediction of Flow Depth and Sediment Discharge in Open Channels*, Rep. KH-R-43A, Calif. Inst. of Technol., Pasadena, Calif.
Cao, S., and T. Tamura (2006), Experimental study on roughness effects on turbulent boundary layer flow over a two-dimensional steep hill, *J. Wind Eng. Ind. Aerodyn.*, *94*(1), 1–19.
Carling, P. A., E. Go, L. La, and U. K. E-mail (2000a), The morphodynamics of fluvial sand dunes in the River Rhine, near Mainz, Germany. I. Sedimentology and morphology, *Sedimentology*, *47*, 227–252.
Carling, P. A., J. J. Williams, E. Gölz, and A. D. Kelsey (2000b), The morphodynamics of fluvial sand dunes in the River Rhine, near Mainz, Germany. II. Hydrodynamics and sediment transport, *Sedimentology*, *47*, 253–278.
Chang, K., and G. Constantinescu (2013), Coherent structures in flow over two-dimensional dunes, *Water Resour. Res.*, *49*, 2446–2460, doi:10.1002/wrcr.20239.
Church, M. (2006), Bed material transport and the morphology of alluvial river channels, *Annu. Rev. Earth Planet. Sci.*, *34*, 325–354.
Coleman, S. E., and V. I. Nikora (2011), Fluvial dunes: Initiation, characterization, flow structure, *Earth Surf. Processes Landforms*, *36*(1), 39–57, doi:10.1002/esp.2096.
Dade, W. B., and P. F. Friend (1998), An empirical model of subcritical bedform migration, *J. Geol.*, *106*(6), 661–676.
Dellil, A. Z., A. Azzi, and B. A. Jubran (2004), Turbulent flow and convective heat transfer in a wavy wall channel, *Heat Mass Transfer*, *40*(10), 793–799.
Einstein, H. A., and N. L. Barbarossa (1952), River channel roughness, *Trans. Am. Soc. Civ. Eng.*, *117*(1), 1121–1132.
Engelund, F., and E. Hansen (1967), *Monograph on Sediment Transport in Alluvial Streams*, Teknisk Forlag, Copenhagen.
Flemming, B. W. (1988), Zur Klassifikation subaquatischer, strömungstransversaler Transportkörper, *Bochumer Geol. Geotech. Arb.*, *29*, 93–97.
Fredsøe, J. (1981), Unsteady flow in straight alluvial streams. Part 2. Transition from dunes to plane bed, *J. Fluid Mech.*, *102*, 431–453.
Gong, W., and A. Ibbetson (1989), A wind tunnel study of turbulent flow over model hills, *Boundary Layer Meteorol.*, *49*(1–2), 113–148.
Gong, W., P. A. Taylor, and A. Dörnbrack (1996), Turbulent boundary-layer flow over fixed aerodynamically rough two-dimensional sinusoidal waves, *J. Fluid Mech.*, *312*, 1–37.
Goring, D. G., and V. I. Nikora (2002), Despiking acoustic Doppler velocimeter data, *J. Hydraul. Eng.*, *128*(1), 117–126, doi:10.1061/(ASCE)0733-9429(2002)128:1(117).
Hendershot, M., J. Venditti, R. Bradley, R. Kostaschuk, M. Church, and M. Allison (2016), Response of low angle dunes to variable flow, *Sedimentology*, doi:10.1111/sed.12236.
Henn, D. S., and R. I. Sykes (1999), Large-eddy simulation of flow over wavy surfaces, *J. Fluid Mech.*, *383*(1), 75–112, doi:10.1017/S0022112098003723.
Husson, D. (2012), RedNoise_ConfidenceLevels, Matlab Cent. File Exch., Retrieved October 22, 2015.
Huthoff, F. (2012), Theory for flow resistance caused by submerged roughness elements, *J. Hydraul. Res.*, *50*(1), 10–17.
Jackson, R. G. (1976), Sedimentological and fluid-dynamic implications of the turbulent bursting phenomenon in geophysical flows, *J. Fluid Mech.*, *77*(3), 531–560, doi:10.1017/S0022112076002243.
Kadota, A., and I. Nezu (1999), Three-dimensional structure of space-time correlation on coherent vortices generated behind dune crest, *J. Hydraul. Res.*, *37*, 59–80.
Kline, S. J., W. C. Reynolds, F. A. Schraub, and P. W. Runstadler (1967), The structure of turbulent boundary layers, *J. Fluid Mech.*, *30*, 741–773, doi:10.1017/S0022112067001740.
Kostaschuk, R. (2006), Sediment transport mechanics and subaqueous dune morphology, in *River, Coast. Estuar. Morphodynamics*, pp. 795–801, Taylor and Francis, London.
Kostaschuk, R., D. Shugar, J. Best, D. Parsons, S. Lane, R. Hardy, and O. Orfeo (2009), Suspended sediment transport and deposition over a dune: Río Paraná, Argentina, *Earth Surf. Processes Landforms*, *34*(12), 1605–1611, doi:10.1002/esp.1847.
Kostaschuk, R. A. (2000), A field study of turbulence and sediment dynamics over subaqueous dunes with flow separation, *Sedimentology*, *47*(3), 519–531, doi:10.1046/j.1365-3091.2000.00303.x.
Kostaschuk, R. A., and M. Church (1993), Macroturbulence generated by dunes: Fraser River, Canada, *Sediment. Geol.*, *85*(1–4), 25–37, doi:10.1016/0037-0738(93)90073-E.
Kostaschuk, R. A., and P. Villard (1996), Flow and sediment transport over large subaqueous dunes: Fraser River, Canada, *Sedimentology*, *43*(5), 849–863, doi:10.1111/j.1365-3091.1996.tb01506.x.
Kostaschuk, R. A., and P. Villard (1999), Turbulent sand suspension over dunes, in *Fluvial Sedimentology VI*, edited by N. D. Smith and J. Rogers, pp. 3–13, Blackwell, Oxford.

Kostaschuk, R. A., J. Best, P. Villard, J. Peakall, and M. Franklin (2005), Measuring flow velocity and sediment transport with an acoustic Doppler current profiler, *Geomorphology*, *68*(1–2), 25–37, doi:10.1016/j.geomorph.2004.07.012.

Kuzan, J. D., T. J. Hanratty, and R. J. Adrian (1989), Turbulent flows with incipient separation over solid waves, *Exp. Fluids*, *7*(2), 88–98.

Kwoll, E., C. Winter, and M. Becker (2013), Intermittent suspension and transport of fine sediment over natural tidal bedforms, in *Coherent Flow Structures at Earth's Surface*, edited by J. G. Venditti et al., pp. 231–242, John Wiley, Chichester.

Kwoll, E., M. Becker, and C. Winter (2014), With or against the tide: The influence of bed form asymmetry on the formation of macroturbulence and suspended sediment patterns, *Water Resour. Res.*, *50*, 7800–7815, doi:10.1002/2013WR014292.

Lefebvre, A., V. B. Ernstsen, and C. Winter (2013), Estimation of roughness lengths and flow separation over compound bedforms in a natural-tidal inlet, *Cont. Shelf Res.*, *61–62*, 98–111, doi:10.1016/j.csr.2013.04.030.

Lefebvre, A., A. J. Paarlberg, and C. Winter (2014), Flow separation and shear stress over angle-of-repose bed forms: A numerical investigation, *Water Resour. Res.*, *50*, 986–1005, doi:10.1002/2013WR014587.

Lin, C. M., and J. G. Venditti (2013), An empirical model of subcritical bedform migration, *Sedimentology*, *60*(7), 1786–1799, doi:10.1111/sed.12056.

Lu, S. S., and W. W. Willmarth (1973), Measurements of the structure of the Reynolds stress in a turbulent boundary layer, *J. Fluid Mech.*, *60*(03), 481–511, doi:10.1017/S0022112073000315.

Lyn, D. (1993), Turbulence measurements in open-channel flows over artificial bed forms, *J. Hydraul. Eng.*, *119*(3), 306–326, doi:10.1061/(ASCE)0733-9429(1993)119:3(306).

Marchioli, C., V. Armenio, M. V. Salvetti, and A. Soldati (2006), Mechanisms for deposition and resuspension of heavy particles in turbulent flow over wavy interfaces, *Phys. Fluids*, *18*(2), 1–16, doi:10.1063/1.2166453.

Matthes, G. H. (1947), Macroturbulence in natural stream flow, *Eos Trans. AGU*, *28*, 255–262, doi:10.1029/TR028i002p00255.

McLean, S. R., J. M. Nelson, and S. R. Wolfe (1994), Turbulence structure over two-dimensional bed forms: Implications for sediment transport, *J. Geophys. Res.*, *99*, 12,729–12,747, doi:10.1029/94JC00571.

McLean, S. R., S. Wolfe, and J. Nelson (1999), Spatially averaged flow over a wavy boundary revisited, *J. Geophys. Res.*, *104*, 743–753.

McLean, S. R., V. I. Nikora, and S. E. Coleman (2008), Double-averaged velocity profiles over fixed dune shapes, *Acta Geophys.*, *56*(3), 669–697, doi:10.2478/s11600-008-0031-0.

Motamedi, A., H. Afzalimehr, J. Gallichand, and E. F. N. Abadi (2012), Lee-angle effects in near bed turbulence: An experimental study on low and sharp angle dunes, *Int. J. Hydraul. Eng.*, *1*(6), 68–74.

Motamedi, A., H. Afzalimehr, V. P. Singh, and L. Dufresne (2014), Experimental study on the influence of dune dimensions on flow separation, *J. Hydrol. Eng.*, *19*(1), 78–86, doi:10.1061/(ASCE)HE.1943-5584.0000754.

Müller, A., and A. Gyr (1986), On the vortex formation in the mixing layer behind dunes, *J. Hydraul. Res.*, *24*(5), 359–375, doi:10.1080/00221688609499314.

Naqshband, S., J. S. Ribberink, D. Hurther, and S. J. M. H. Hulscher (2014), Bed load and suspended load contributions to migrating sand dunes in equilibrium, *J. Geophys. Res. Earth Surf.*, *119*, 1043–1063, doi:10.1002/2013JF003043.

Nelson, J. M., and J. D. Smith (1989), Mechanics of flow over ripples and dunes, *J. Geophys. Res.*, *94*, 8146–8162, doi:10.1029/JC094iC06p08146.

Nelson, J. M., S. McLean, and S. Wolfe (1993), Mean flow and turbulence fields over two-dimensional bed forms, *Water Resour. Res.*, *29*, 3935–3953, doi:10.1029/93WR01932.

Nezu, I., and H. Nakagawa (1993), *Turbulence in Open-Channel Flows*, edited by International Association for Hydraulic Research, Balkema, Rotterdam.

Nikora, V., D. Goring, I. McEwan, and G. Griffiths (2001), Spatially averaged open-channel flow over rough bed, *J. Hydraul. Eng.*, *127*(2), 123–133, doi:10.1061/(ASCE)0733-9429(2001)127:2(123).

Ogink, H. J. M. (1989), Hydraulic roughness over single and compound bedforms, *Rep. 1314-XI/Q786*, Delft Hydraulics, Delft.

Omidyeganeh, M., and U. Piomelli (2011), Large-eddy simulation of two-dimensional dunes in a steady, unidirectional flow, *J. Turbul.*, *12*(N42), 1–31.

Paarlberg, A. J., C. M. Dohmen-Janssen, S. J. M. H. Hulscher, and P. Termes (2007), A parameterization of flow separation over subaqueous dunes, *Water Resour. Res.*, *43*, W12417, doi:10.1029/2006WR005425.

Paarlberg, A. J., C. M. Dohmen-Janssen, S. J. M. H. Hulscher, and P. Termes (2009), Modeling river dune evolution using a parameterization of flow separation, *J. Geophys. Res.*, *114*, F01014, doi:10.1029/2007JF000910.

Paarlberg, A. J., C. M. Dohmen-Janssen, S. J. M. H. Hulscher, P. Termes, and R. Schielen (2010), Modelling the effect of time-dependent river dune evolution on bed roughness and stage, *Earth Surf. Processes Landforms*, *35*(15), 1854–1866.

Parsons, D. R., J. L. Best, O. Orfeo, R. J. Hardy, R. Kostaschuk, and S. N. Lane (2005), Morphology and flow fields of three-dimensional dunes, Rio Paraná, Argentina: Results from simultaneous multibeam echo sounding and acoustic Doppler current profiling, *J. Geophys. Res.*, *110*, F04S03, doi:10.1029/2004JF000231.

Roden, J. E. (1998), The sedimentology and dynamics of mega-dunes, Jamuna River, Bangladesh, Doctoral Dissertation, Univ. of Leeds, Leeds.

Rood, K. M., and E. J. Hickin (1989), Suspended-sediment concentration and calibre in relation to surface-flow structure in Squamish River estuary, southwestern British Columbia, *Can. J. Earth Sci.*, *26*(10), 2172–2176, doi:10.1139/e89-183.

Ruck, B., and B. Makiola (1990), Flow over a single-sided backward facing step with step angle variations, in *Laser Anemometry—Advances and Applications*, edited by J. T. Turner, pp. 369–378, Springer, Berlin.

Ruck, B., and B. Makiola (1993), Flow separation over the inclined step, in *Physics of Separated Flows—Numerical, Experimental and Theoretical Aspects*, *Notes on Numer. Fluid Mech. 40*, edited by K. Gersten, pp. 47–55, Springer Vieweg, Wiesbaden.

Saunderson, H. C., and F. P. J. Lockett (1983), Flume experiments on bedforms and structures at the dune-plane bed transition, in *Modern and Ancient Fluvial Systems*, *Int. Assoc. Sedimentol. Spec. Publ.*, vol. 6, pp. 49–58, Blackwell Sci., Oxford.

Schindler, R. J., and A. Robert (2005), Flow and turbulence structure across the ripple-dune transition: An experiment under mobile bed conditions, *Sedimentology*, *52*(3), 627–649, doi:10.1111/j.1365-3091.2005.00706.x.

Schmeeckle, M. W. (2014), Numerical simulation of turbulence and sediment transport of medium sand, *J. Geophys. Res. Earth Surf.*, *119*, 1240–1262, doi:10.1002/2013JF002911.

Shugar, D. H., R. A. Kostaschuk, J. L. Best, D. R. Parsons, S. N. Lane, O. Orfeo, and R. J. Hardy (2010), On the relationship between flow and suspended sediment transport over the crest of a sand dune, Río Paraná, Argentina, *Sedimentology*, *57*(1), 252–272, doi:10.1111/j.1365-3091.2009.01110.x.

Simpson, R. (1989), Turbulent boundary-layer separation, *Annu. Rev. Fluid Mech.*, *21*, 205–234.

Simpson, R. L. (1996), Aspects of turbulent boundary-layer separation, *Prog. Aerosp. Sci.*, *32*, 457–521.

Smith, J. D., and S. R. McLean (1977), Spatially averaged flow over a wavy surface, *J. Geophys. Res.*, *82*, 1735–1746, doi:10.1029/JC082i012p01735.

Stoesser, T., C. Braun, M. García-Villalba, and W. Rodi (2008), Turbulence structures in flow over two-dimensional dunes, *J. Hydraul. Eng.*, *134*(1), 42–55, doi:10.1061/(ASCE)0733-9429(2008)134:1(42).

Sukhodolov, A. N., J. J. Fedele, and B. L. Rhoads (2006), Structure of flow over alluvial bedforms: An experiment on linking field and laboratory methods, *Earth Surf. Processes Landforms*, *31*(10), 1292–1310, doi:10.1002/esp.1330.

Tennekes, H., and J. L. Lumley (1972), *A First Course in Turbulence*, MIT Press, Cambridge, Mass.

Thomson, D. J. (1982), Spectrum estimation and harmonic analysis, *Proc. IEEE*, *70*(9), 1055–1096.

TSI Incorporated (2005), *Phase Doppler Particle Analyzer (PDPA)/ Laser Doppler Velocimeter (LDV) TSI*, Shoreview, Minn.

Vanoni, V. A., and N. H. Brooks (1957), Laboratory studies of the roughness and suspended load of alluvial streams, *Rep. E-68*, Calif. Inst. Technol., Pasadena, Calif.

Van Rijn, L. C. (1993), *Principles of Sediment Transport in Rivers, Estuaries and Coastal Seas*, Aqua Publ., Amsterdam.

Venditti, J. G. (2007), Turbulent flow and drag over fixed two- and three-dimensional dunes, *J. Geophys. Res.*, *112*, F04008, doi:10.1029/2006JF000650.

Venditti, J. G. (2013), Bedforms in sand-bedded rivers, in *Treatise on Geomorphology*, edited by J. Shroder and E. Wohl, pp. 137–162, Academic Press, San Diego, Calif.

Venditti, J. G., and S. S. J. Bennett (2000), Spectral analysis of turbulent flow and suspended sediment transport over fixed dunes, *J. Geophys. Res.*, *105*, 22,035–22,047, doi:10.1029/2000JC900094.

Venditti, J. G., M. Church, and S. J. Bennett (2005), On the transition between 2D and 3D dunes, *Sedimentology*, *52*(6), 1343–1359, doi:10.1111/j.1365-3091.2005.00748.x.

Wan, Z., and Z. Y. Wang (1994), *Hyperconcentrated Flow*, A. A. Balkema, Rotterdam.

Warmink, J. J., M. J. Booij, H. Van der Klis, and S. J. M. H. Hulscher (2013), Quantification of uncertainty in design water levels due to uncertain bed form roughness in the Dutch river Waal, *Hydrol. Processes*, *27*(11), 1646–1663, doi:10.1002/hyp.9319.

Wilbers, A. (2004), The development and hydraulic roughness of subaqueous dunes, Doctoral Dissertation, Uetrecht Univ., Uetrecht.

Wilkinson, R. H. (1984), A method for evaluating statistical errors associated with logarithmic velocity profiles, *Geo-Mar. Lett.*, *3*(1), 49–52.

Winter, C., M. Chiou, R. Riethmüller, V. B. Ernstsen, D. Hebbeln, and B. W. Flemming (2006), The concept of "representative tides" in morphodynamic numerical modelling, *Geo-Mar. Lett.*, *26*(3), 125–132, doi:10.1007/s00367-006-0031-5.

Wood, N. (1995), The onset of separation in neutral, turbulent flow over hills, *Boundary Layer Meteorol.*, *76*(1–2), 137–164, doi:10.1007/BF00710894.

Wren, D. G., R. A. Kuhnle, and C. G. Wilson (2007), Measurements of the relationship between turbulence and sediment in suspension over mobile sand dunes in a laboratory flume, *J. Geophys. Res.*, *112*, F03009, doi:10.1029/2006JF000683.

Yalin, M. S. (1972), *Mechanics of Sediment Transport*, Pergamon Press, Oxford.

Yoon, H. S., O. A. El-Samni, A. T. Huynh, H. H. Chun, H. J. Kim, A. H. Pham, and I. R. Park (2009), Effect of wave amplitude on turbulent flow in a wavy channel by direct numerical simulation, *Ocean Eng.*, *36*(9–10), 697–707, doi:10.1016/j.oceaneng.2009.03.012.

Yue, W. S., C. L. Lin, and V. C. Patel (2006), Large-eddy simulation of turbulent flow over a fixed two-dimensional dune, *J. Hydraul. Eng.*, *132*(7), 643–651, doi:10.1061/(asce)0733-9429(2006)132:7(643).

Zilker, D. P., and T. J. Hanratty (1979), Influence of the amplitude of a solid wavy wall on a turbulent flow. Part 2. Separated flows, *J. Fluid Mech.*, *90*(2), 257–271.

Zilker, D. P., G. W. Cook, and T. J. Hanratty (1977), Influence of the amplitude of a solid wavy wall on a turbulent flow. Part 1. Non-separated flows, *J. Fluid Mech.*, *82*(1), 29–51.